Supplement of Atmos. Chem. Phys., 18, 15261–15289, 2018
https://doi.org/10.5194/acp-18-15261-2018-supplement

Atmospheric Chemistry and Physics
Open Access
EGU

Supplement of

Large simulated radiative effects of smoke in the south-east Atlantic

Hamish Gordon et al.

Correspondence to: Hamish Gordon (hamish.gordon@cern.ch)

Supplementary materials for: Large simulated radiative effects of smoke in the south-east Atlantic

Hamish Gordon[1], Paul R. Field[1,2], Steven J. Abel[2], Ben T. Johnson[2], Mohit Dalvi[2], Daniel P. Grosvenor[1], Adrian A. Hill[2], Annette K. Miltenberger[1], Masaru Yoshioka[1], and Ken S. Carslaw[1]

1. School of Earth and Environment, University of Leeds, LS2 9JT, United Kingdom

2. Met Office, Fitzroy Road, Exeter, EX1 3PB, United Kingdom

Supplementary 1: satellite intercomparison

The LWP from SEVIRI is calculated using the formula

$$\frac{2}{3}\tau_{vis} r_e \rho_l \tag{S1}$$

where the cloud optical thickness τ_{vis} is retrieved at $1.6\,\mu\mathrm{m}$; r_e is the effective radius, also retrieved at $1.6\,\mu\mathrm{m}$, and ρ_l is the density of liquid water (Roebeling et al., 2008a). For MODIS the same equation is used except for multiplication by a factor $2/Q_e$, where $Q_e \sim 2$ is the extinction efficiency (King et al., 2013).

The cloud droplet number N_d is calculated from MODIS data using the equation

$$N_d = \frac{\sqrt{5}}{2k\pi} \frac{(f * C_w * \tau_{vis})^{1/2}}{Q \rho_l r_e^{5/2}} \tag{S2}$$

where $k = 0.8$, $Q = 2$, $f = 0.7$, and C_w is the rate of increase of liquid water content with height (Boers et al., 2006; Grosvenor and Wood, 2014),

$$C_w = \frac{C_p}{L_v} \left(\Gamma_d - \Gamma_m\right) \rho_a \tag{S3}$$

. In this last equation, Γ_d and Γ_m are the dry and moist adiabatic lapse rates, C_p the heat capacity of dry air, ρ_a its density, and L_v the latent heat of condensation of water. The SEVIRI calculation is similar (Roebeling et al., 2008b).

Table S1. Comparison of optical retrievals: normalized mean bias (b) and Pearson correlation coefficient (r) of SEVIRI relative to MODIS AQUA. The data are all regridded to the coarser AMSR resolution, to avoid artefacts from slight mis-alignment of the model grids.

Day	R_e b	R_e r	COT b	COT r	N_d b	N_d r
1	-0.20	0.53	-0.29	0.59	-0.34	0.64
2	-0.24	0.68	-0.20	0.93	-0.28	0.63
3	-0.22	0.71	-0.18	0.82	-0.31	0.83
4	-0.40	0.71	-0.34	0.90	+0.08	0.77
5	-0.34	0.64	-0.16	0.79	+0.41	0.53
6	-0.37	0.83	-0.19	0.93	+0.33	0.54
7	-0.25	0.59	-0.15	0.95	-0.07	0.55
8	-0.12	0.24	+0.01	0.66	-0.46	0.35
9	-0.13	0.60	-0.29	0.86	-0.47	0.71
10	-0.06	0.82	-0.28	0.68	-0.47	0.77

Table S2. Comparison of liquid water path retrievals: normalized mean bias (b) and Pearson correlation coefficient (r) of MODIS AQUA and SEVIRI relative to AMSR, on the AMSR resolution.

Day	AQUA b	AQUA r	SEV b	SEV r
1	-0.23	0.48	-0.37	0.16
2	-0.12	0.69	-0.32	0.63
3	-0.31	0.64	-0.41	0.58
4	-0.11	0.61	-0.46	0.48
5	-0.15	0.49	-0.42	0.43
6	-0.02	0.77	-0.48	0.74
7	-0.14	0.65	-0.37	0.65
8	-0.23	0.49	-0.21	0.38
9	-0.15	0.67	-0.21	0.61
10	-0.12	0.32	-0.11	0.47

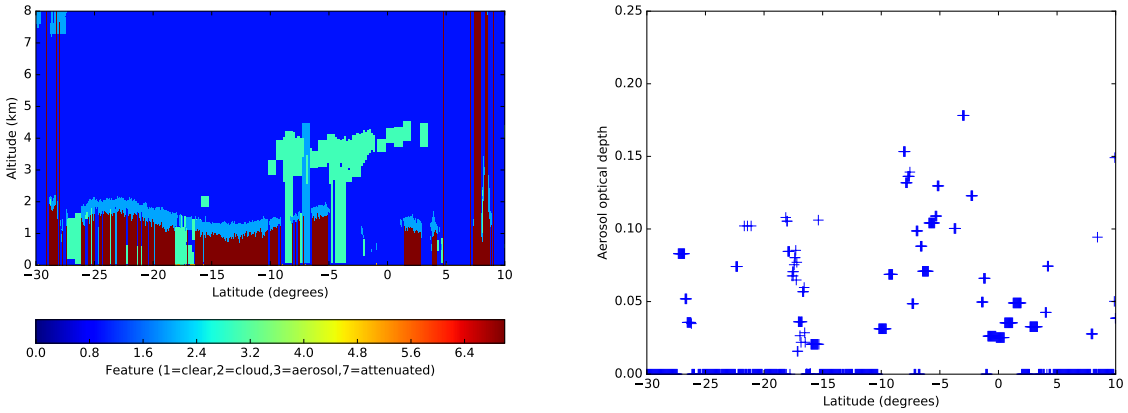

Figure S1. CALIOP vertical feature mask and aerosol optical depth (filtered such that the AOD uncertainty is below 0.05) for 7 August (the left plot is identical to the bottom subplot of Figure 4).

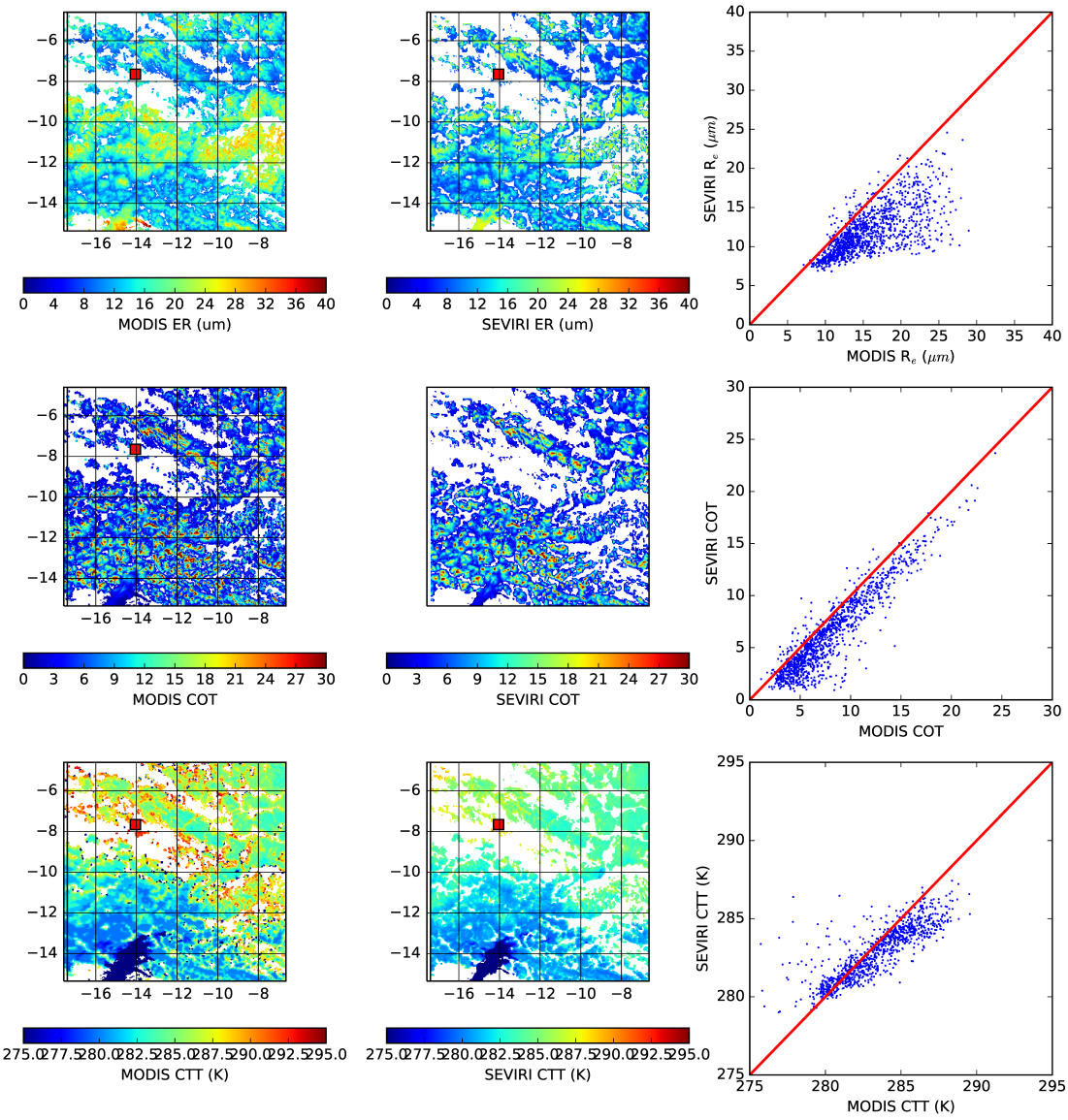

Figure S2. MODIS (left) and SEVIRI (centre) cloud droplet effective radius (at $3.7\,\mu\mathrm{m}$, cloud optical thickness, and cloud top temperature, on 2nd August 2016, and the correlation of coarse-grained values (in AMSR $14\,\mathrm{km}$ grid boxes), right. Liquid water paths below $10\,\mathrm{g\,m^{-2}}$ are screened out, for clarity. Summary statistics for all ten days of the study period are given in Table S1 below.

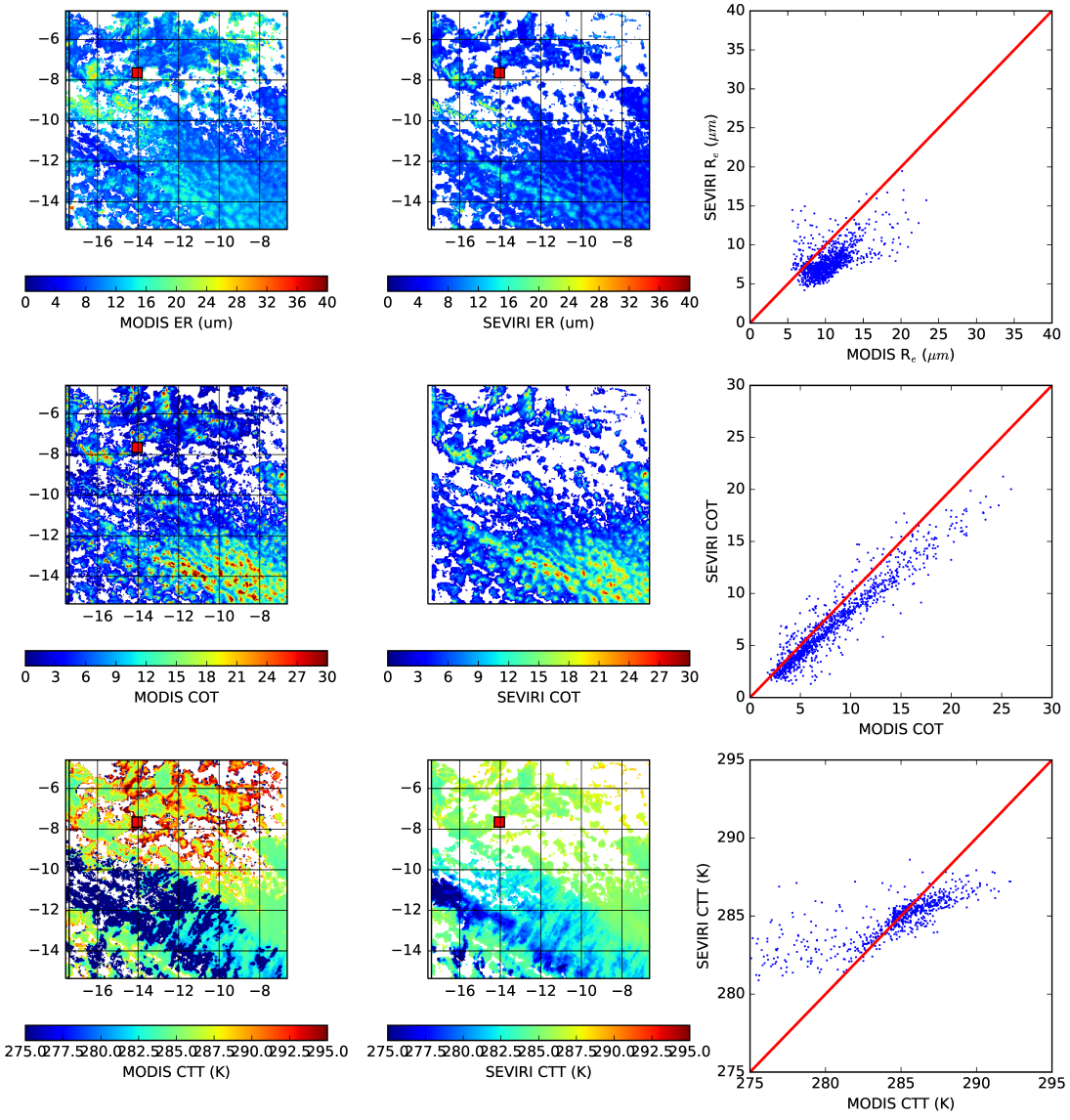

Figure S3. MODIS (left) and SEVIRI (centre) cloud droplet effective radius, cloud optical thickness, and cloud top temperature, on 7th August 2016, and the correlation of coarse-grained values (in AMSR 14 km grid boxes), right. Liquid water paths below $10\,\mathrm{gm}^{-2}$ are screened out, for clarity.

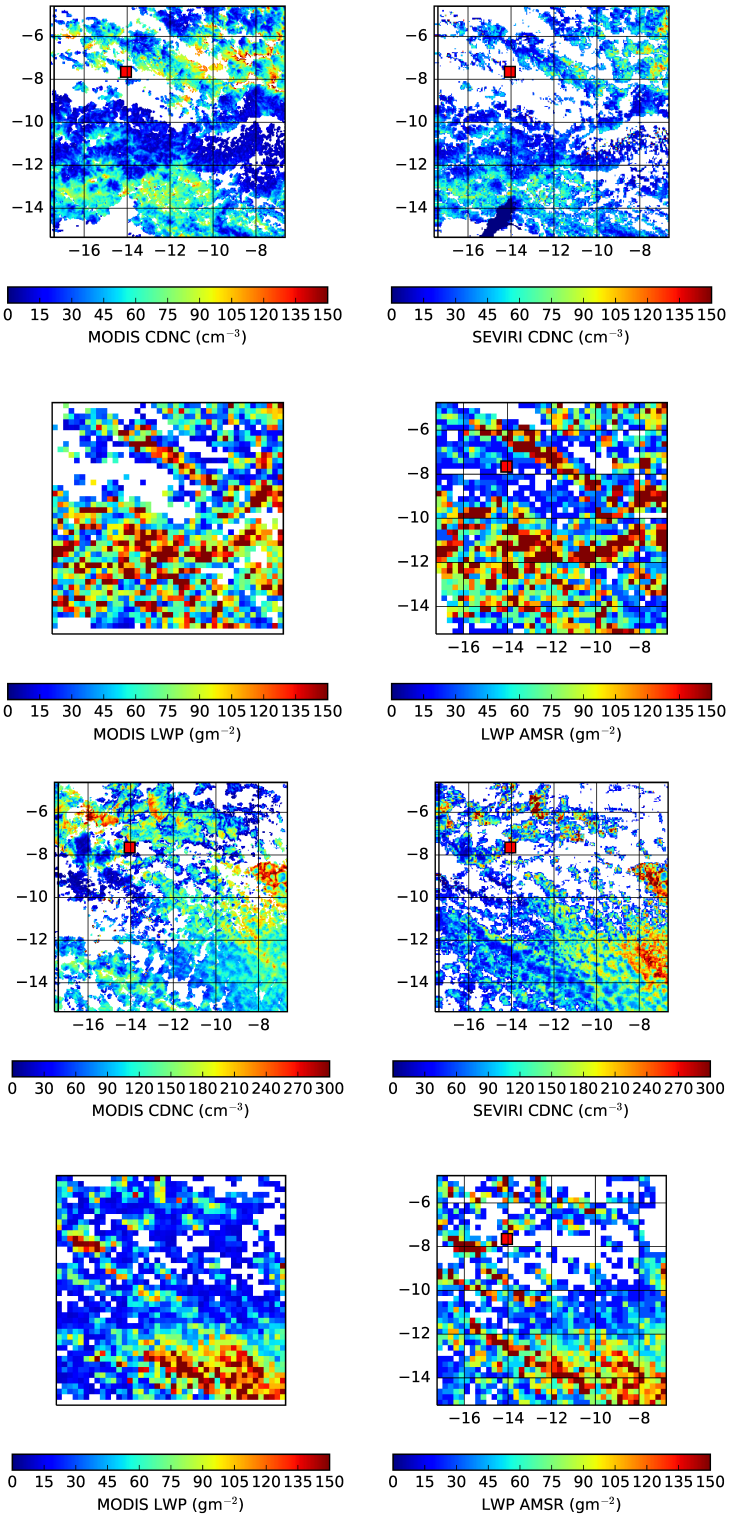

Figure S4. MODIS cloud droplet number concentration and liquid water path (left) on 2nd and 7th August 2016, and, right, SEVIRI cloud droplet number concentration and AMSR liquid water path.

Supplementary 2: additional simulation output

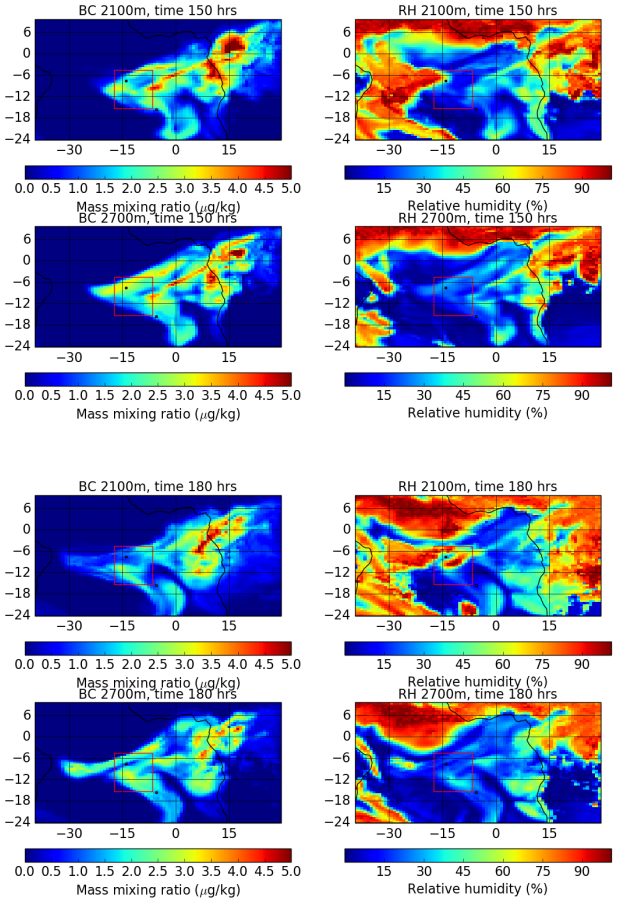

Figure S5. Black carbon mass loading (left) and relative humidity (right) at the specified altitudes, 150 (top) and 180 (bottom) hours into the simulation.

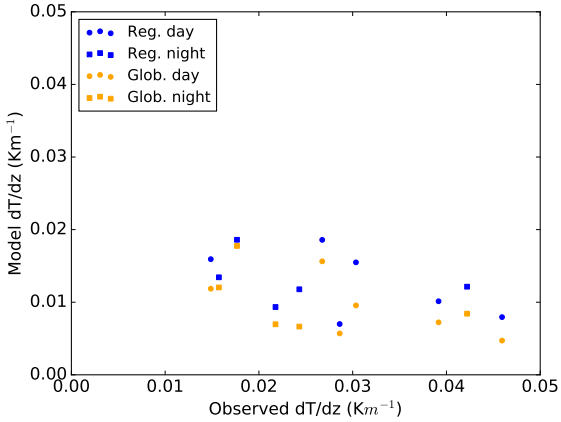

Figure S6. Temperature gradient across the inversion at Ascension Island in the radiosonde observations from the ARM site (D. Holdridge, J. Kyrouac and R. Coulter, 2016b), plotted against the values from the model. The difference between the maximum and minimum temperatures around the inversion is divided by the difference in height between these extrema.

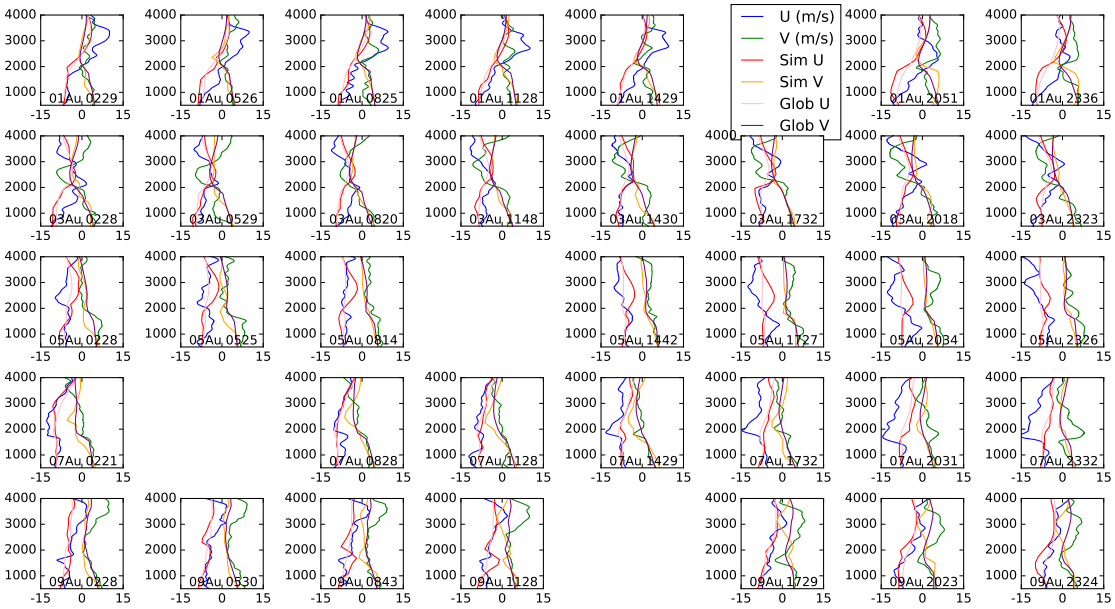

Figure S7. Observed and modelled wind speed profiles at Ascension Island, from soundings on 1,3,5,7,9 August (D. Holdridge, J. Kyrouac and R. Coulter, 2016b). Wind speed is plotted on the x axis and altitude in metres on the y axis of each sub-plot. The soundings are compared to the regional simulation, marked as 'Sim U' and 'Sim V'.

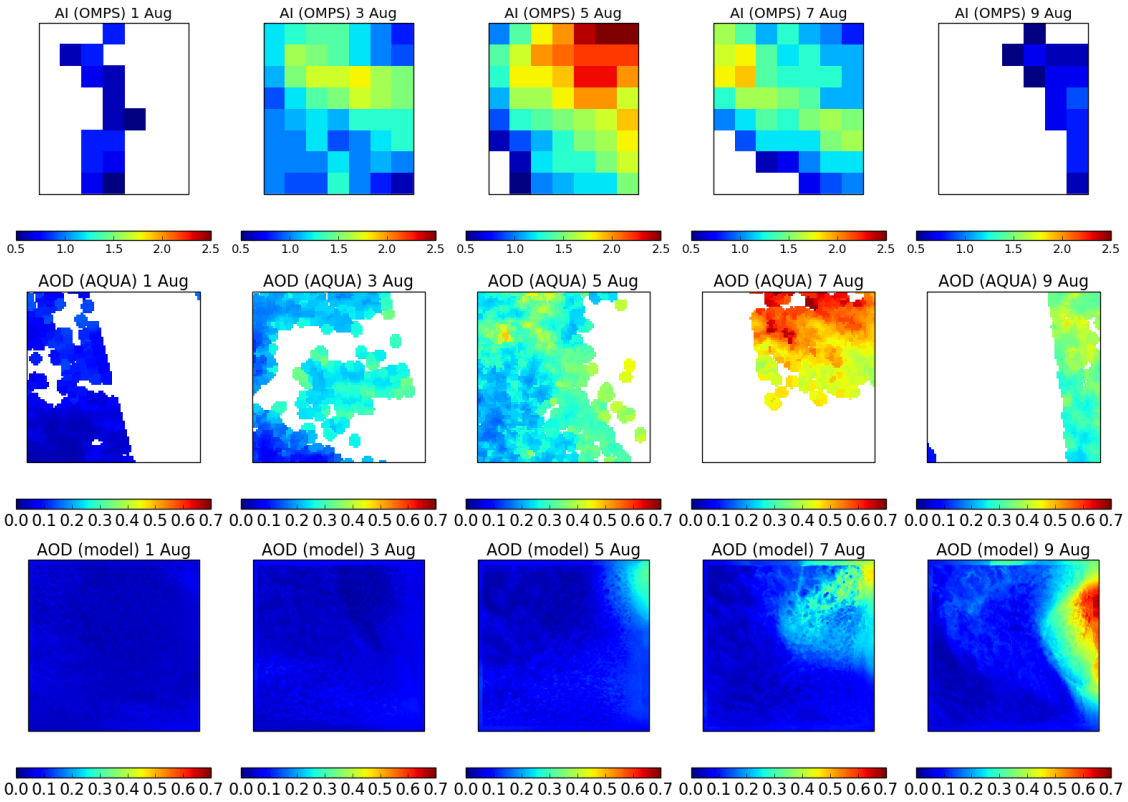

Figure S8. Aerosol index (top) from OMPS, aerosol optical depth (AOD) from MODIS AQUA (middle) and AOD from the regional model (bottom) on 1,3,5,7,9 August. The MODIS AOD is filtered to exclude regions above cloud, before being regridded to the model grid. The regridding algorithm excludes cloudy regions, white on the plots, where valid AOD retrievals are greater than 0.25° (28 km) apart (we assume that AOD is slowly varying on lengthscales smaller than this, so a retrieval will be representative of neighbouring areas where cloud is beneath the aerosol). The aerosol index is only retrieved from OMPS if it is greater than around 0.5.

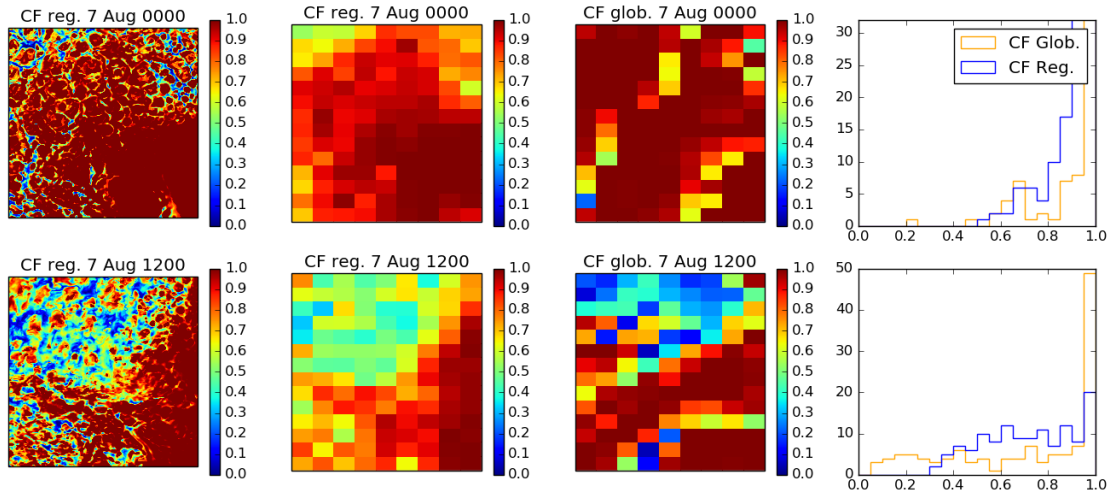

Figure S9. Cloud fractions from the Unified Model cloud schemes at 0130 UTC(top) and 1330 UTC (bottom) on 7 August. The left plot shows the regional model, then the regional model regridded onto the global grid, then the global model, and finally the histogram of cloud fractions in model grid boxes. In all plots the maximum cloud fraction in an atmospheric column is shown.

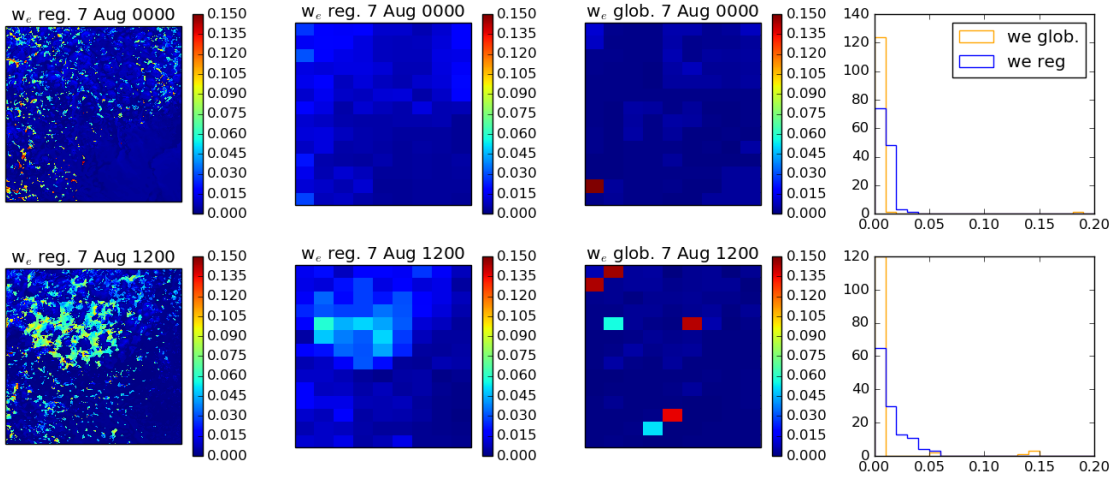

Figure S10. Entrainment rates at the top of the boundary layer at 0130 UTC(top) and 1330 UTC (bottom) on 7 August. The left plot shows the regional model, then the regional model regridded onto the global grid, then the global model, and finally the histogram of entrainment rates in model grid boxes.

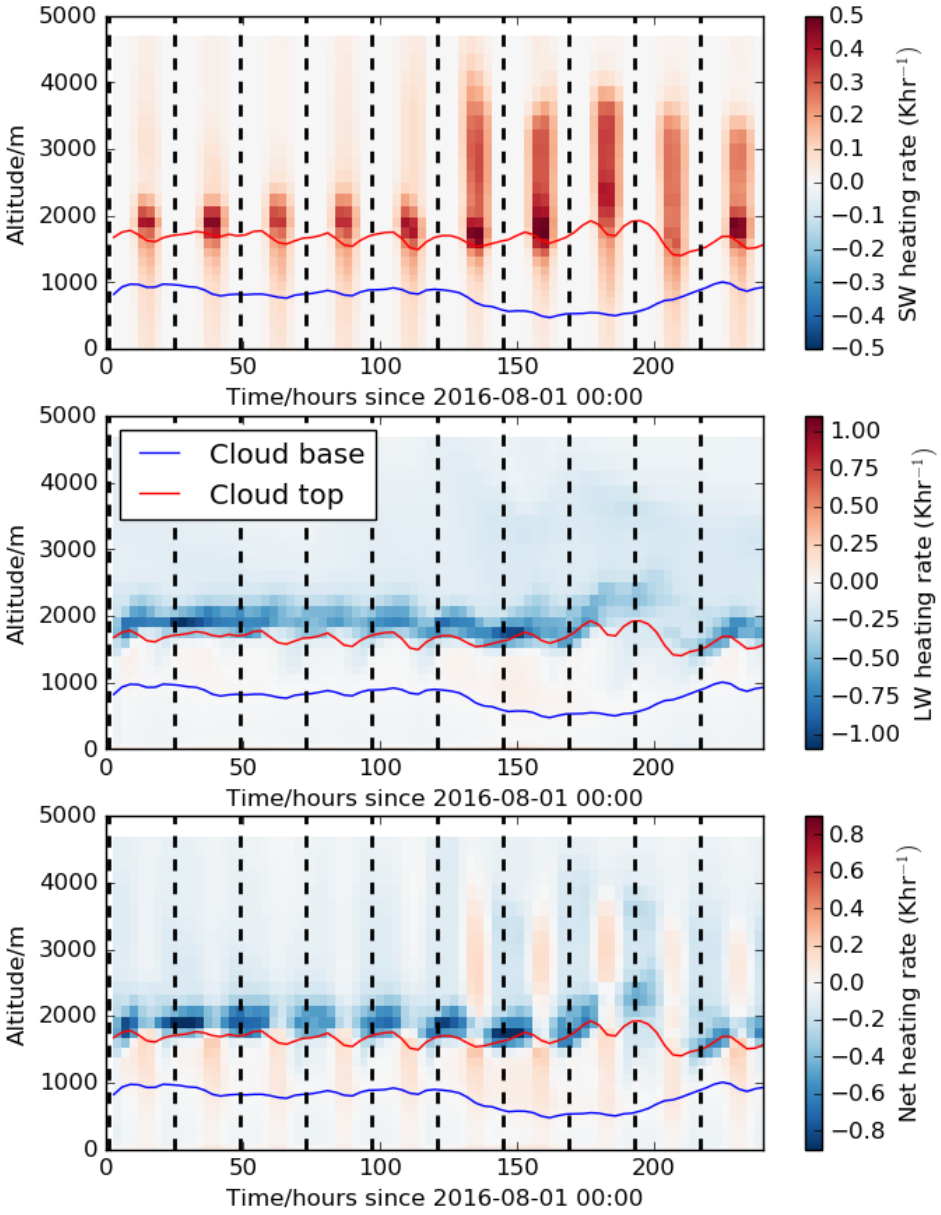

Figure S11. Shortwave, longwave and net domain mean heating rates during the ten-day model simulation in the regional model. The dotted vertical lines indicate midnight, local time. Cloud base and cloud top are also marked.

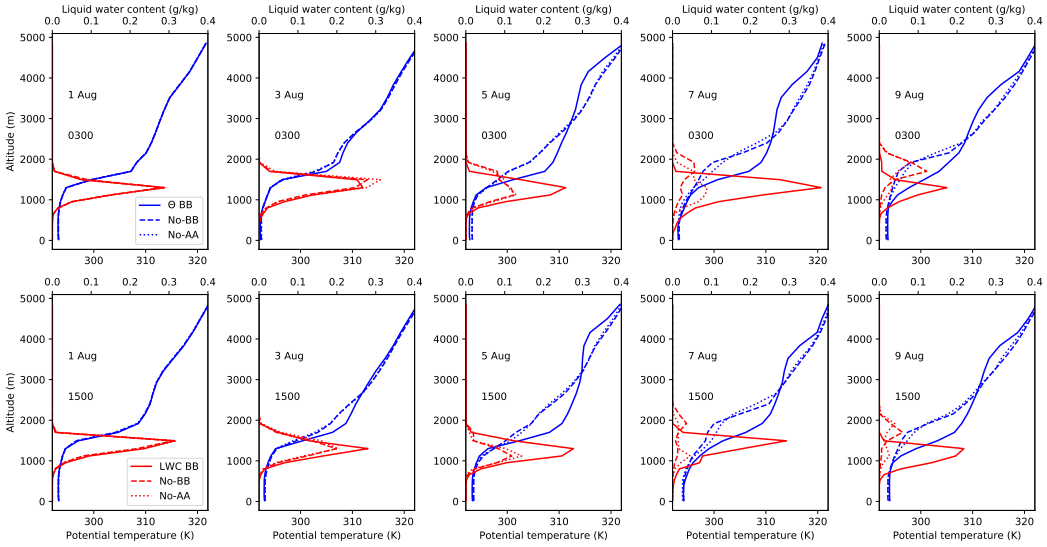

Figure S12. Domain-mean vertical profiles of potential temperature Θ and liquid water content (LWC) with and without biomass burning aerosol on odd numbered days at the times of day marked, from the global model.

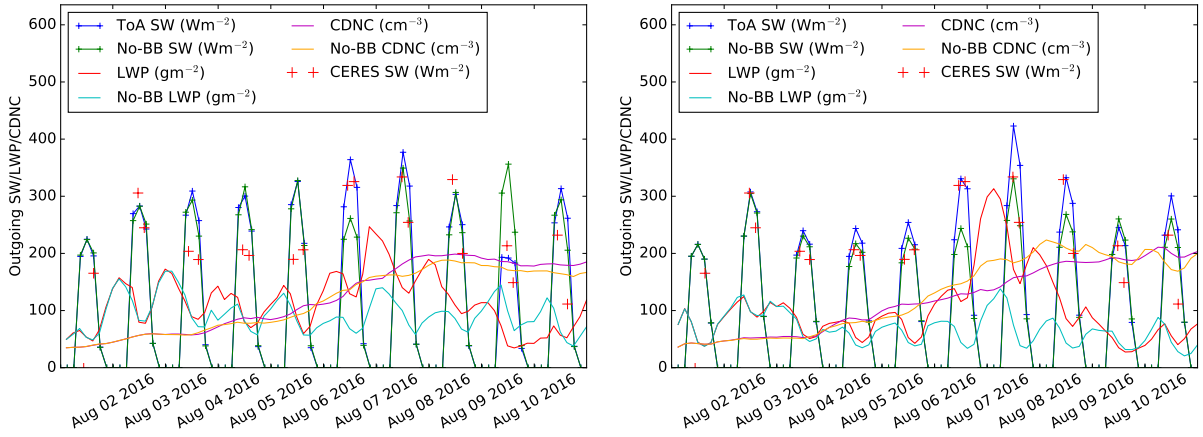

Figure S13. Outgoing shortwave flux at top of atmosphere for the baseline model and a model version with aerosol absorption set to zero, for the regional domain in the global model on the left and the regional model on the right. CERES domain-mean observations are shown in the same figure in red crosses (some of these may be biased due to the gaps between swaths). The changes to CDNC and liquid water path across the 10 days are also shown.

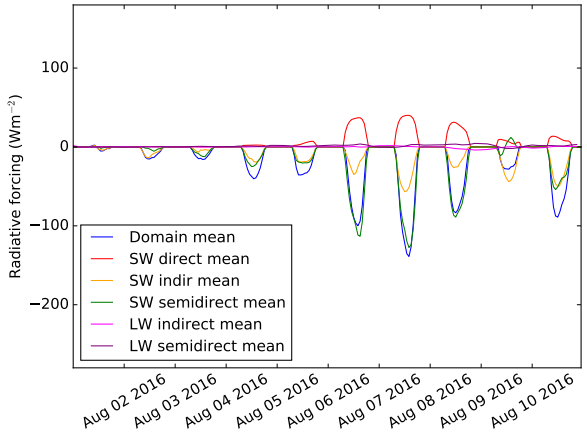

Figure S14. Decomposition of the short-wave and long-wave radiative effects of biomass burning aerosol using simulations with the micro-physical parameterisation of Kogan (2013) instead of the default, from Khairoutdinov and Kogan (2000).

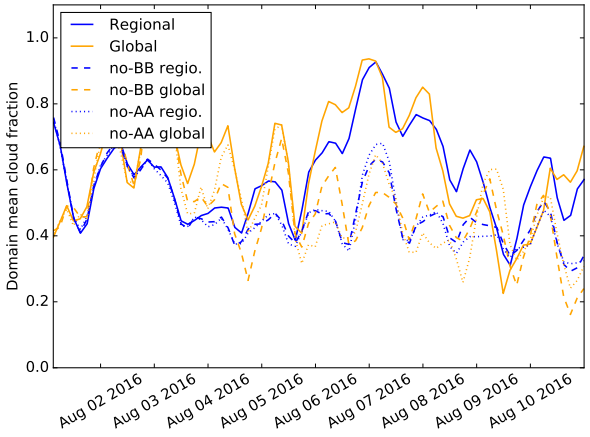

Figure S15. Cloud fraction with and without biomass burning emissions in the regional model, and in the same domain in the global model. The simulations without aerosol absorption are also shown.

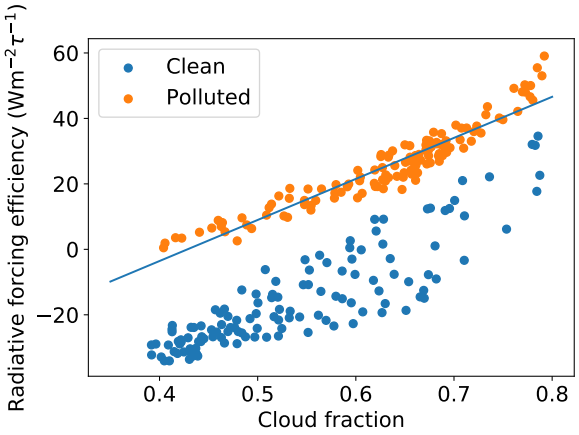

Figure S16. Radiative forcing efficiency (Chand et al., 2009), defined as the direct effect divided by the aerosol optical depth, as a function of cloud fraction f_c in the clean and polluted periods of our regional model simulation. The linear fit shown for the polluted period has equation $125.4 f_c - 53.7$.